ISSN 8755-6839

SCIENCE OF **TSUNAMI HAZARDS**

Journal of Tsunami Society International

Volume 29 **Number 2** **2010**

FLOW AND POTENTIAL FORCE DUE TO RUNUP TSUNAMI AROUND A COASTAL FOREST WITH A GAP – EXPERIMENTS AND NUMERICAL SIMULATIONS

Nguyen Ba Thuy [a], Katsutoshi Tanimoto [b], Norio Tanaka [c, *]

[a] Graduate School of Science and Engineering, Saitama University, 255 Shimo-okubo, Sakura-ku, Saitama, 338-8570, Japan.
[b] Emeritus Professor of Saitama University, 255 Shimo-okubo, Sakura-ku, Saitama 338-8570, Japan.
[c,*] Professor, Institute for Environmental Science and Technology, Saitama University, 255 Shimo-okubo, Sakura-ku, Saitama 338-8570, Japan.
Tel./Fax: +81-48-858-3564. E-mail address: tanaka01@mail.saitama-u.ac.jp

ABSTRACT

In the present study, laboratory experiments were conducted to validate the applicability of numerical model based on two-dimensional nonlinear long-wave equations including drag resistance of trees and turbulence induced shear forces to tsunami flow around a simplified forest with a gap in a wave channel. It was confirmed that the water surface elevation and flow velocity by the numerical simulations agree well with the experimental results for various forest conditions of width and tree density. Then the numerical model was applied to a prototype scale condition of a coastal forest of *Pandanus odoratissimus* with a gap to investigate the effects of forest conditions (width and tree density) and incident tsunami conditions (period and height) on a potential tsunami force. The potential tsunami force at the gap exit is greatly enhanced and the maximum in the spatial distribution around and inside the forest. The potential tsunami forces at four representative points at front and back of forest including the center of gap exit were analyzed for various conditions and formulated as function of forest and tsunami conditions in the non-dimensional form. The potential tsunami forces calculated by the curve-fit formula agree well with the simulated potential tsunami forces within ±10% error.

Key words: Runup tsunami, Coastal forest, Gap, *Pandanus odoratissimus*, Tsunami force

1. INTRODUCTION

Since the Indian Ocean tsunami in 2004, numerous studies have elucidated the effects of coastal vegetation in reducing tsunami forces and the damage to humans and property based on post-tsunami surveys (for example, Danielsen et al. 2005; Kathiresan and Rajendran, 2005; Tanaka et al., 2007). Currently, coastal forests are widely considered to be effective for mitigating tsunami damage from both economic and environmental points of view, although their role is still questioned due to the absence of adequate studies (Kerr and Baird, 2007). In fact, several projects to plant vegetation on coasts as a bioshield against tsunamis have been started in South and Southeast Asian countries (Tanaka et al., 2009; Tanaka, 2009).

The reduction in tsunami damage behind a coastal forest depends on the vegetation species and their dimensions (tree height, diameter, and density), scale and arrangement of the forest (along-shore length and cross-shore width), and tsunami conditions. In relation to forest arrangement, Mascarenhas and Jayakumar (2008) pointed out that roads perpendicular to the beach in a coastal forest served as a passages for a tsunami to travel inland in many places in Tamil Nadu-India on the occasion of the 2004 Indian Ocean tsunami. Fernando et al. (2008) reported that the destruction of coral by the tsunami was remarkable in some places in Hikkaduwa and Akuralla in Sri Lanka, and that the inundation depth behind the destroyed coral reefs was much larger than that behind unbroken coral reefs. Fernando et al. (2008) also conducted a laboratory experiment to verify the effect of an open gap in submerged porous barriers and found that the flow velocity at the gap exit was significantly higher than the case with no gap. Although the latter case was not a coastal forest, those indicate a negative effect of a gap in tsunami runup.

Tanaka et al. (2007) pointed out that *Pandanus odoratissimus*, which is dominant coastal vegetation in South and Southeast Asia, is especially effective in providing protection from tsunami damage due to its density and complex aerial root structure. To study the effect of a gap in a coastal forest of *P. odoratissimus*, Nandasena et al. (2008) performed a numerical simulation including resistance by the forest for limited conditions and found that a narrow gap has a significant effect on the exit flow, but an insignificant effect on the runup height. Thuy et al. (2009a) conducted experiments on a costal forest with a gap by using a simplified model in a 0.4-m-wide wave channel and validated that the numerical results, including the turbulence-induced shear force in addition to the forest resistance, agreed well with experimental results for both runup height and velocity at the gap exit. They also applied the numerical model to a coastal forest of *P. odoratissimus* with a gap and found that a 15-m-wide gap caused the highest velocity under their calculated conditions of a fixed condition of incident tsunami. Based on the discussions in experiment and prototype scale, they confirmed that the turbulence induced shear force gives a significant effect on the flow velocity at the gap exit. Furthermore, Thuy et al. (2009b) discussed the effects of forest and incident tsunami conditions on inundation depth and flow velocity at the gap exit and behind the vegetation patch based on the numerical results.

The tsunami forces are directly related with the damage of trees and other obstacles; however, tsunami forces were not discussed in previous studies using numerical simulations mentioned above. In the present paper, potential tsunami forces due to runup tsunami around a coastal forest of *P. odoratissimus* with a gap are studied by numerical simulations. The potential tsunami force is defined

as the total drag force on a virtual high column with unit width and unit drag coefficient. The numerical model is based on two-dimensional nonlinear long-wave equations incorporating drag resistance of trees and the sub-depth scale (*SDS*) turbulence model by Nadaoka and Yagi (1998). Laboratory experiments on tsunami flow around a simplified forest model with various width and tree density are conducted in a wave channel to validate the applicability of numerical model. The numerical model is then applied to a prototype scale condition of coastal forest of *P. odoratissimus* with a gap to investigate the effects of forest conditions (width and tree density) and incident tsunami conditions (height and period) on the potential tsunami forces. The potential tsunami forces at four representative points at front and back of forest including the center of gap exit are analyzed and formulated in the non-dimensional form.

2. MATHEMATICAL MODEL AND NUMERICAL METHOD

2.1. Governing equations

The governing equations are two-dimensional nonlinear long-wave equations that include drag and eddy viscosity forces due to interaction with vegetation. The continuity and the momentum equations are respectively:

$$\frac{\partial \zeta}{\partial t} + \frac{\partial (dV_x)}{\partial x} + \frac{\partial (dV_y)}{\partial y} = 0 \tag{1}$$

$$\frac{\partial V_x}{\partial t} + V_x \frac{\partial V_x}{\partial x} + V_y \frac{\partial V_x}{\partial y} + g\frac{\partial \zeta}{\partial x} + \frac{\tau_{bx}}{\rho d} + \frac{F_x}{\rho d} - \frac{E_{Vx}}{d} = 0 \tag{2}$$

$$\frac{\partial V_y}{\partial t} + V_x \frac{\partial V_y}{\partial x} + V_y \frac{\partial V_y}{\partial y} + g\frac{\partial \zeta}{\partial y} + \frac{\tau_{by}}{\rho d} + \frac{F_y}{\rho d} - \frac{E_{Vy}}{d} = 0 \tag{3}$$

where,

$$\vec{\tau}_b = \frac{\rho g n^2}{d^{1/3}} \vec{V} \left| \vec{V} \right| \tag{4}$$

$$\vec{F} = \gamma \frac{1}{2} \rho C_{D-all} b_{ref} \vec{V} \left| \vec{V} \right| d \tag{5}$$

$$E_{vx} = 2\frac{\partial}{\partial x}\left(d\nu_e \frac{\partial V_x}{\partial x} \right) + \frac{\partial}{\partial y}\left(d\nu_e \frac{\partial V_x}{\partial y} + d\nu_e \frac{\partial V_y}{\partial x} \right) \tag{6}$$

$$E_{vy} = 2\frac{\partial}{\partial y}\left(d\nu_e \frac{\partial V_y}{\partial y} \right) + \frac{\partial}{\partial x}\left(d\nu_e \frac{\partial V_x}{\partial y} + d\nu_e \frac{\partial V_y}{\partial x} \right) \tag{7}$$

x and y are the horizontal coordinates; V_x and V_y are the depth-averaged velocity components in x and y directions respectively; t is the time; d the total water depth ($d=h+\zeta$); h the local still water depth (on land, the negative height of the ground surface); ζ the water surface elevation; g the gravitational acceleration; ρ the water density; n the Manning roughness coefficient; γ the tree density (number of trees/m^2). $C_{D\text{-}all}$ is the depth-averaged equivalent drag coefficient considering the vertical stand structure of the trees, which was defined by Tanaka et al. (2007) as:

$$C_{D-all}(d) = C_{D-ref}\frac{1}{d}\int_0^d \frac{b(z_G)}{b_{ref}}\frac{C_D(z_G)}{C_{Dref}})dz_G \tag{8}$$

where $b(z_G)$ and $C_D(z_G)$ are the projected width and drag coefficient of a tree at height z_G from the ground surface, and b_{ref} and $C_{D\text{-}ref}$ are the reference width of the trunk and the reference drag coefficient at breast height, respectively. The eddy viscosity v_e is given by the *SDS* turbulence model as described below.

2.2. Turbulence model

The *SDS* turbulence model of Nadaoka and Yagi (1998) was applied to evaluate the eddy viscosity with modifications related to the bottom friction and vegetation resistance.

$$\frac{\partial k_D}{\partial t} + V_x\frac{\partial k_D}{\partial x} + V_y\frac{\partial k_D}{\partial y} = \frac{1}{d}\frac{\partial}{\partial x}\left(d\frac{v_e}{\sigma_k}\frac{\partial k_D}{\partial x}\right) + \frac{1}{d}\frac{\partial}{\partial y}\left(d\frac{v_e}{\sigma_k}\frac{\partial k_D}{\partial y}\right) + p_{kh} + p_{kv} + p_{kd} - \varepsilon_D \tag{9}$$

$$p_{kh} = v_e\left[2\left(\frac{\partial V_x}{\partial x}\right)^2 + \left(\frac{\partial V_x}{\partial y} + \frac{\partial V_y}{\partial x}\right)^2 + 2\left(\frac{\partial V_y}{\partial y}\right)^2\right] \tag{10}$$

$$p_{kv} = \frac{gn^2}{d^{4/3}}(V_x^2 + V_y^2)^{1.5} \tag{11}$$

$$p_{kd} = \frac{\gamma b_{ref} C_{D-all}}{2}(V_x^2 + V_y^2)^{1.5} \tag{12}$$

$$\nu_e = c_w\frac{k_D^2}{\varepsilon_D} \tag{13}$$

$$\varepsilon_D = c_d \frac{k_D^{1.5}}{l_D} \tag{14}$$

where k_D is the kinetic energy and $l_D = \lambda d$ is the length scale (λ : turbulence length scale coefficient). For the model parameters, standard values are adopted: c_w=0.09, c_d=0.17, σ_k=1.0 and λ=0.08.

2.3. Method of numerical simulations

A set of the above equations is solved by the finite-difference method of a staggered leap-frog scheme, which is widely used in numerical simulations of tsunami (for example, Liu et al., 1994; Titov and Synolakis, 1997; Imamura et al., 1998; Koh et al., 2009). An upwind scheme was used for nonlinear convective terms in order to maintain numerical stability. A semi-Crank–Nicholson scheme was used for the terms of bed friction, drag, and turbulence-induced shear force. On the offshore sides, a wave generation zone with a constant water depth in which the governing equations were reduced to linear long-wave equations was introduced to achieve non-reflective wave generation by using the method of characteristics. A sinusoidal incident tsunami was given as a time-dependent boundary condition at the most offshore side of the wave-generation zone. For a moving boundary treatment, a number of algorithms were necessary so that the flow occurring when the water surface elevation is high enough can flow to the neighboring dry cells. The initial conditions were given for a waveless state in the computational domain including the wave-generation zone.

3. EXPERIMENTS AND VALIDATION OF NUMERICAL MODEL

3.1. Experimental setup and conditions

The present experiments are follow-up from Thuy et al. (2009a) in which the effect of gap width on flow around a simplified forest model of vertical cylinders with a fixed width and tree density was investigated by a fixed condition of long waves in a wave channel with 0.4 m wide. It was found that a 0.07 m-wide gap causes the largest velocity at the gap exit under their conditions. In this study, the effects of forest conditions on the flow velocity and water surface elevation at the gap exit and behind the vegetation patch are mainly investigated.

Fig. 1 shows the experimental setup in the wave channel where the forest model was set in the water area for the convenience of velocity measurements. Trees were simply modeled by wooden cylinders with a diameter of 0.005 m mounted in a staggered arrangement as seen in Fig. 2. The gap width b_G was fixed as 0.07 m in the present experiments. The forest width B_F was changed in cases of 0.2, 0.5, 0.7 and 1.0 m with the fixed density of 2200 trees/m^2 (0.22 trees/cm^2). The end of forest was fixed at x=11.36 m (see Fig. 1), where the still water depth is 0.037 m. Three cases of tree density for the fixed forest width of 1.0 m were tested; lower density (γ=500 tree/m^2), moderate density (γ=1000 trees/m^2), and higher density (γ=2200 trees/m^2). In addition to those cases, experiments for cases of no forest (B_F=γ=0) and full vegetation (no gap) were also conducted. Wave condition was fixed as that the incident wave height H_i at still water depth of 0.44 m is 0.02 m and the wave period T is 20 s as same as the previous experiments (Thuy et al., 2009a).

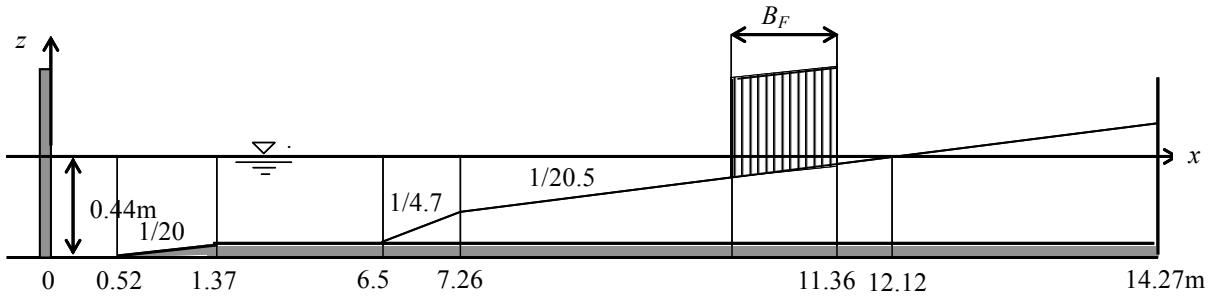

Fig. 1. Experimental setup in wave channel.

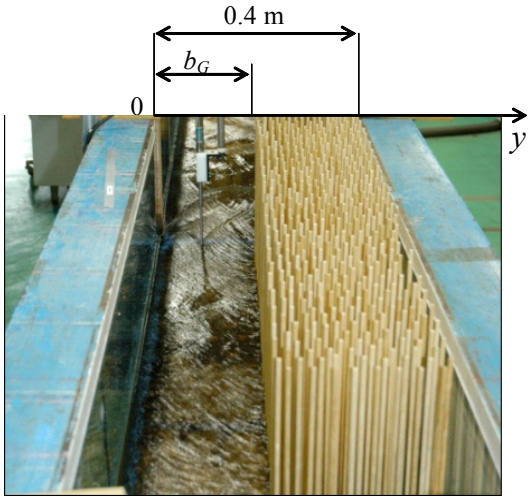

Fig. 2. Photo of forest model (example of b_G=0.15 m).

3.2. Conditions of numerical simulation for laboratory scale

For numerical simulations of the experimental conditions, the uniform grid size of 0.005 m and time step of 0.002 s were selected. The Manning roughness coefficient n was given as 0.012 s/m$^{1/3}$ for the relatively rough wooden bottom. For parameters in the turbulence model, standard values as indicated in *2.2.* were applied. The drag coefficient $C_{D\text{-}ref}$ depends on both the Reynolds number and relative spacing of vegetation (s/D), where s is the distance between cylinders and D is the diameter of cylinder. However, Chakrabati (1991) showed that the interaction between multiple cylinders becomes small when s/D is larger than 2, and the drag coefficient of multiple cylinders approaches to a single cylinder. In the present experimental conditions, the drag coefficient may be assumed as a single

cylinder because the s/D is considerably greater than 2. The drag coefficient C_{Dref} was determined to be 1.5 after some trial calculations, which is consistent with the drag coefficient of a circular cylinder in the laboratory scale corresponding to the Reynolds number of 300.

The measurements of water surface elevation and horizontal velocity in the experiments were made in a steady state in multi-reflection system of wave channel between reflective wave paddle and coastal model with forest. Consequently, the incident wave height in the numerical simulations must be given with consideration of the effect of reflected waves. Fig. 3 shows examples of wave height measured at six locations in cases of no vegetation and full vegetation. In the figure, two distributions simulated with the incident wave height H_i of 0.02 m are plotted for the actual channel length and for the channel length extended by 21 m, which corresponds to a half of wavelength at the still water depth of 0.44 m. Both results coincide well as the difference is not observed in the figure, because of non-reflective wave generation in the numerical simulations. The simulated distributions also agree well with measured wave heights and the separated incident wave heights on the basis of small amplitude theory at the extended channel are about 0.02 m. Therefore, H_i =0.02 m can be considered as the incident wave height at the still water depth of 0.44 m in the multi-reflection system of wave channel in the present experimental conditions.

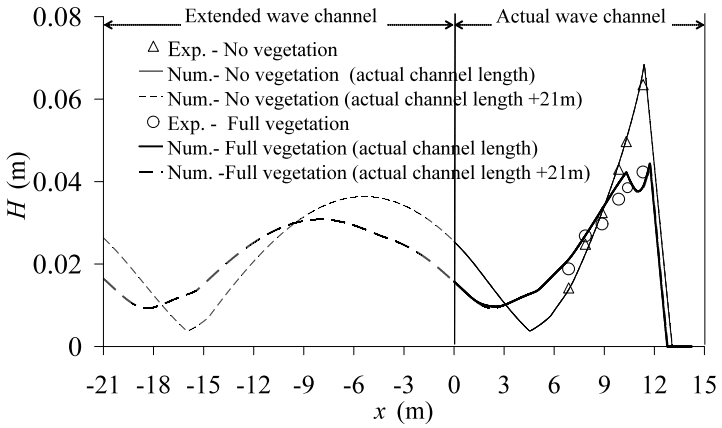

Fig. 3. Wave height distributions in wave channel.

Fig. 4 shows examples of time variation of velocity at the center of vegetation end (y=0.235 m) and the center of gap exit (y=0.035 m) at x=11.4 m during the analyzed time interval of measurements. It is confirmed that the flow velocity is almost steady and the simulated maximum value in particular agrees well with the measured maximum values as already shown in the previous study (Thuy et al., 2009a). The velocity is defined by the following equation because the tsunami flow dominated in the direction of the x-axis in the present study:

$$V = \mathrm{sign}(V_x)\left|\vec{V}\right| \tag{15}$$

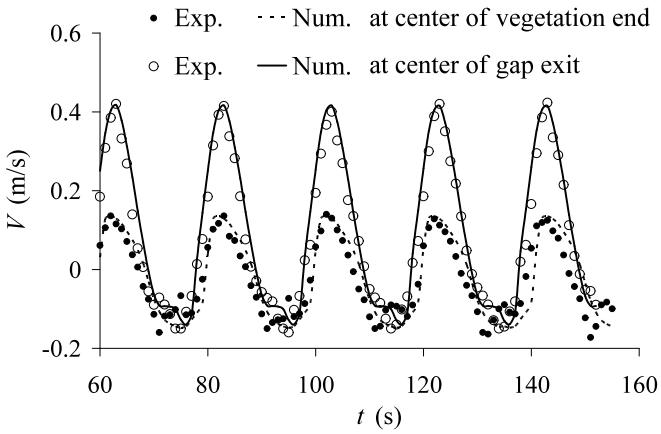

Fig. 4. Time variations of flow velocity (b_G=0.07 m).

3.3. Validation of numerical model with respect to forest conditions

Fig. 5 shows the distribution of maximum velocity in y-direction at the forest end (x=11.4m) for three cases of tree density. The change of velocity gradient around the edge of gap is remarkable, which suggests the importance of turbulence induced shear force at the gap as already discussed by Thuy et al. (2009a). It is also noted that the increase in tree density reduces the velocity behind the vegetation patch, whereas it increases in the velocity at the gap exit. Those are fairly well realized in the present numerical model simulations.

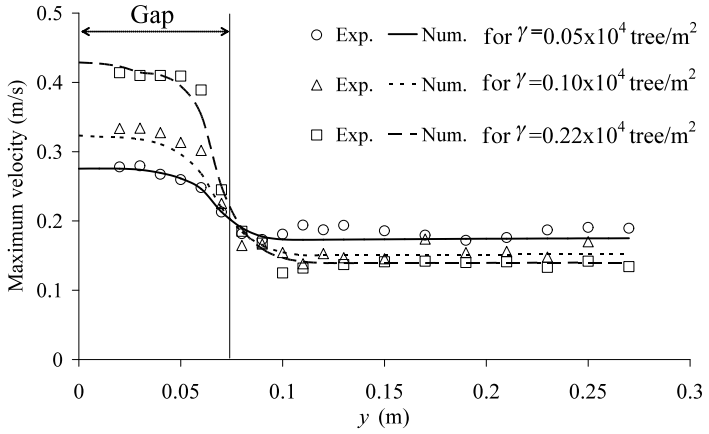

Fig. 5. Distribution of maximum velocity (x=11.4 m).

Fig. 6 shows the variation of the change of wave crest (ζ_{max}), maximum velocity at the gap exit (V_{Gmax}) and maximum velocity at the center behind the vegetation patch (V_{VPmax}) against the forest width. The wave crest and velocity behind the vegetation patch decreases and the maximum velocity at the gap exit increases as forest width increases. The numerical results agree fairly well with the experimental results.

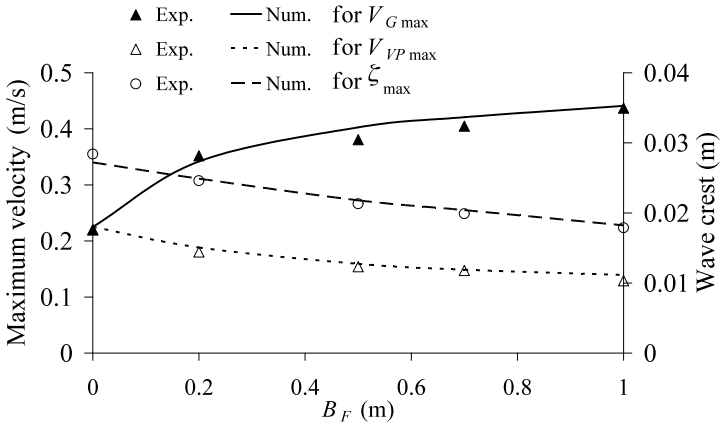

Fig. 6. Effect of forest width on maximum velocity and wave crest height.

4. EFFECT OF FOREST AND TSUNAMI CONDITIONS ON POTENTIAL TSUNAMI FORCES IN ACTUAL SCALE

4.1. Topography, forest and tsunami conditions, and definitions of potential tsunami force

4.1.1. Topography and forest conditions

A uniform coastal topography with the cross-shore section perpendicular (x-axis) to a straight shoreline, as shown in Fig.7 (a), was selected as a model case. The bed profile of the domain consists of four slopes, S=1/10, 1/100, 1/50, and 1/500. The offshore water depth at an additional wave-generation zone with a horizontal bottom is 100 m below the datum level of z=0. The tide level at the attack of the tsunami was considered to be 2 m, and therefore the still water level is 2 m above the datum level. The direction of the incident tsunami is perpendicular to the shoreline.

The coastal forest starts at the starting point of the 1/500 slope on the land (x=5700 m), where the ground is 4 m above the datum level (2 m above the tide level at the tsunami event). The forest was assumed to extend in the direction of the shoreline (y-axis) with the arrangement of a gap and vegetation patches with an along-shore unit length of L_F and a cross-shore width of B_F, as shown in Fig. 7(b). Both side boundaries, shown by dot-and-dash lines in the figure, are mirror image axes in which no cross flow exists. A gap with a width b_G is perpendicular to the shoreline and located at the center of the along-shore forest length. In the present study, the forest length L_F and gap width b_G were fixed as 200 m and 15 m respectively. The forest width B_F was changed from 0 m (no forest) to

200 m for selected cases, and the forest width of 1000 m was additionally considered in order to investigate an extreme condition. According to Thuy et al. (2009a), the forest (L_F=200 m) is long enough to avoid the effect of a gap around the mirror image boundary, so that tsunami flow becomes one-dimensional there as in the case of coastal forest without a gap. In the numerical simulations, the uniform grid size of 2.5 m was applied. In Fig. 7(b), representative checkpoints of simulated results are shown as A (x=5700+B_F+1.25 m, y=100 m), B (x=5700+B_F+1.25 m, y=156.25 m), C (x=5701.25 m, y=108.75 m) and D (x=5701.25 m, y=156.25 m). The Manning roughness coefficient n was set as 0.025 s/m$^{1/3}$ for a relatively rough bare ground, which is widely used in numerical simulations of tsunami runup (for example, Harada and Imamura, 2005).

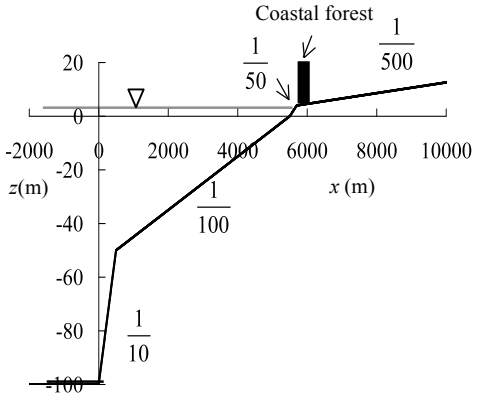

(a)

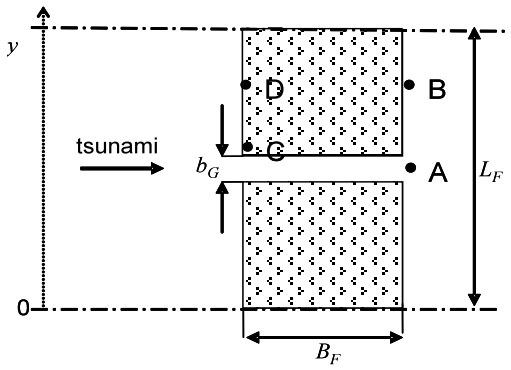

(b)

Fig. 7. Schematic topography. (a) Cross section, (b) sketch of forest and gap arrangement.

In the present study, a coastal forest consisting of *P. odoratissimus* was considered. As shown in Fig. 8(a), *P. odoratissimus* has a complex aerial root structure that provides additional stiffness and increases the drag coefficient. Fig. 8(b) shows the $b(z_G)/b_{ref}$, $C_D(z_G)/C_{Dref}$, and $C_{D\text{-}all}$ of *P. odoratissimus* based on Tanaka et al. (2007) for the conditions of the tree height H_{Tree}=8 m (for a mature tree), the reference diameter b_{ref}=0.195 m. The reference drag coefficient $C_{D\text{-}ref}$ of 1.0 was adopted for a trunk with a circular section and a rough surface in the region of high Reynolds number. The value of $C_{D\text{-}all}$ varied with the total depth d (inundation depth) because the projected width b and the drag coefficient C_D vary with the height from the ground surface z_G as shown in the figure. The tree density γ was changed from 0 (no forest) to 0.4 trees/m^2 in numerical simulations.

(a)

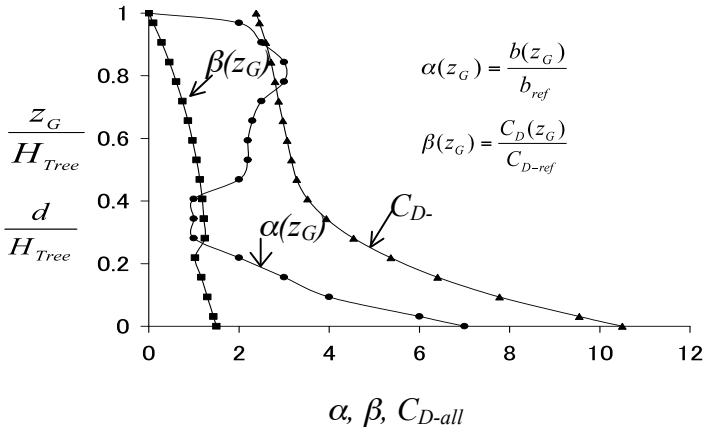

(b)

Fig. 8. Characteristics of *P. odoratissimus*. (a) Photographs of a stand, and (b) vertical distribution of α, β, and $C_{D\text{-}all}$.

4.1.2. Tsunami conditions

As already described, the tsunami attack on the coast is perpendicular to the shoreline at a tide level of 2 m. An incident tsunami at the offshore boundary is a sinusoidal wave starting positive with period T and height H_i from 600 to 3600 s and from 2 to 8 m, respectively. In the present paper, the runup of only the first wave was analyzed because it has the largest runup height among continuous waves.

The incident tsunami height (H_i) at the offshore boundary is rather arbitrary because the offshore boundary may be set at an arbitrary depth. Therefore, the tsunami height (H_{sl0}) above the ground surface at the shoreline was used instead of H_i and called the 'incident tsunami height' for the simplicity in the present paper. The range of H_{sl0} is from 3.08 to 8.51 m corresponding to H_i=2 to 8 m with T=1200 s. Note that the suffix 0 in the present paper indicates the absence of a coastal forest.

Fig. 9 shows the spatial distributions of water surface elevation ζ, mean velocity V and $\sqrt{gd}$ of the first runup wave of T=1200 s and H_i=6 m without forest at the time when the water surface elevation at the shoreline is the maximum as H_{sl0}=6.94 m. It is apparent that the runup tsunami is no more like a sinusoidal wave but a bore-like wave and the front is a super-critical flow.

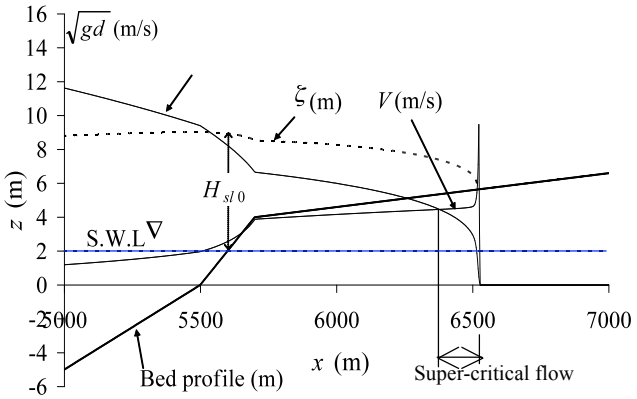

Fig. 9. Spatial distribution of runup tsunami (T=1200 s, H_i=6 m) in the case of no forest at the time when the water surface elevation at the shoreline is the maximum.

4.1.3. Summary of combined conditions of forest and tsunami

Table 1 summarizes combined condition of forest and tsunami in the numerical simulations.

Table 1. Summary of all simulation cases for combined conditions of forest and tsunami.

Series	B_F (m)	γ (trees/m^2)	H_{sl0} (m)	T (s)
Change of forest conditions				
1	0–200, 1000	0.226	6.94	1200
2	100	0–0.4	6.94	1200
Change of tsunami conditions				
3	100	0.226	3.08–8.51	1200
4	100	0.226	6.94	600–3600
Change of tree density and tsunami conditions				
5	100	0.05	4.21–7.73	1200
6	100	0.05	6.94	600–3600
7	100	0.1	4.21–7.73	1200
8	100	0.1	6.94	600–3600
Change of forest width and tsunami conditions				
9	20	0.226	4.21–7.73	1200
10	20	0.226	6.94	600–3600
11	50	0.226	4.21–7.73	1200
12	50	0.226	6.94	600–3600

4.1.4. Definition of a potential tsunami force and the time variation

The tsunami force vector ($\vec{F}^*$) in the present paper is defined by the following equation:

$$\vec{F}^* = \frac{1}{2}\rho d\vec{V}\left|\vec{V}\right| \tag{16}$$

This is a potential tsunami force integrated over the inundation depth and corresponds to the total drag force due to the tsunami acting on a virtual tall column of unit width and a unit drag coefficient. For an example, the integrated drag force vector ($\vec{F}_{Tree}$) on a single tree with a height of H_{Tree} can be calculated by the following relationship:

$$\begin{aligned} \vec{F}_{Tree} &= C_{D-all} b_{ref} \vec{F}^*, \qquad H_{Tree} \geq d \\ &= C_{D-all} b_{ref} \frac{H_{Tree}}{d} \vec{F}^*, \quad H_{Tree} < d \end{aligned} \tag{17}$$

Similarly, the total drag force on a human body as an application may be calculated with appropriate $C_{D\text{-}all}$ and b_{ref} specified to the human body.

Fig. 10 shows the time variations of inundation depth d, mean velocity V, tsunami force F^* for the condition of B_F=100 m, γ=0.226 trees/m^2, H_{sl0}=6.94 m and T=1200 s at the representative checkpoint C. As observed in the figure, the temporal maxima appear at different times. In particular, the maximum of V appeared early in the tsunami arrival when the inundation depth is low, and consequently, the tsunami force was not maximal. Therefore, the representative inundation depth and velocity are defined as values at the time of the temporal maxima of tsunami force ($F^*_{\max}$; hereafter, simply called 'tsunami force'). They are denoted as $d_{F*\max}$, $V_{F*\max}$.

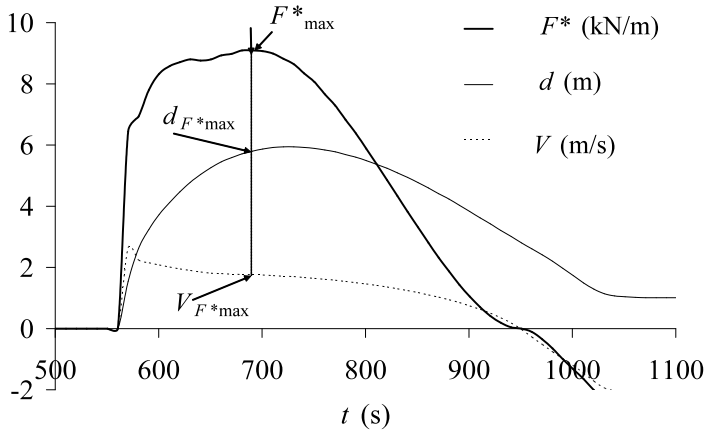

Fig. 10. Time profiles of inundation depth (d), mean velocity (V) and tsunami force (F*) at C.

4.2. Results and discussions

4.2.1. Overview of tsunami runup around forest

In this section, the tsunami runup around a forest with a width of 100 m and a density of 0.226 trees/m^2 is summarized as an example for the incident tsunami conditions of T=1200 s and H_{sl0}=6.94 m. Fig. 11(a) and (b) show the x-y distributions of the maximum inundation depth $d_{\max}$ and the representative inundation depth $d_{F*\max}$, respectively. The distribution of the maximum inundation depth decreases monotonously from about 6 m at the front of the forest to about 3.5 m at the back of the forest. The distribution of the representative inundation depths for the maximum tsunami force is different from that of the maximum inundation depth. In particular, the representative inundation depth in front of the forest is small as 2–3 m. This is because the maximum tsunami force occurred early in the tsunami's arrival and the velocity at the time of the maximum inundation depth was reduced by reflected waves from the forest.

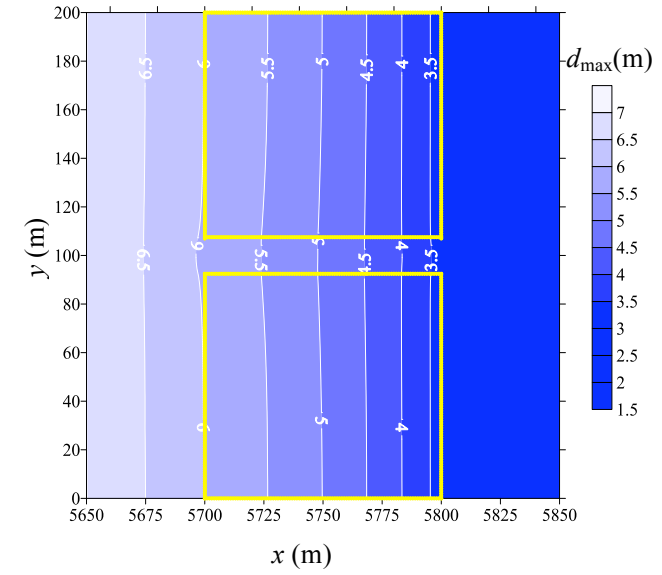

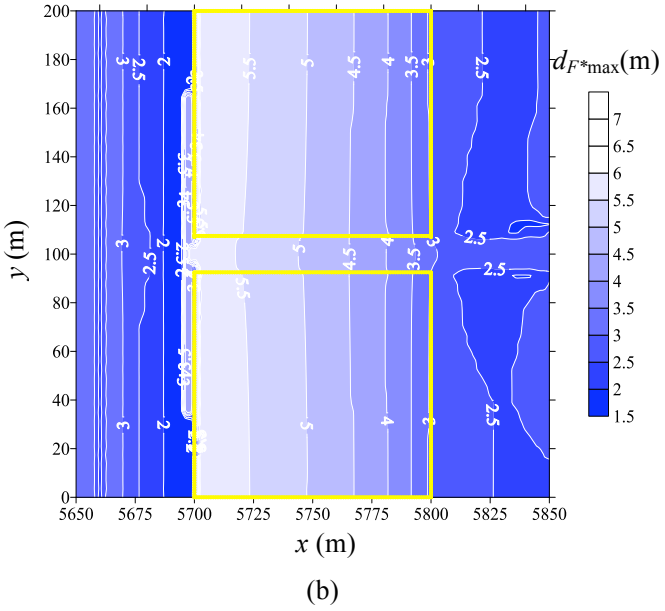

Fig. 11. Distributions of (a) maximum inundation depth (d_{max}), and (b) representative inundation depth (d_{F*max}).

Fig. 12 (a) and (b) show the distributions of the maximum and representative velocity, respectively. As already pointed out by Thuy et al. (2009a), the velocity increased in the gap and became large around the gap exit. The spatial maximum appears behind the gap exit and exceeds 7.5 m/s in the temporal maximum velocity and 7.0 m/s in the representative velocity for the maximum tsunami force. Fig. 13

shows the distributions of the maximum tsunami force. The spatial maximum tsunami force appears at the gap exit (checkpoint A) and exceeds 75 kN/m.

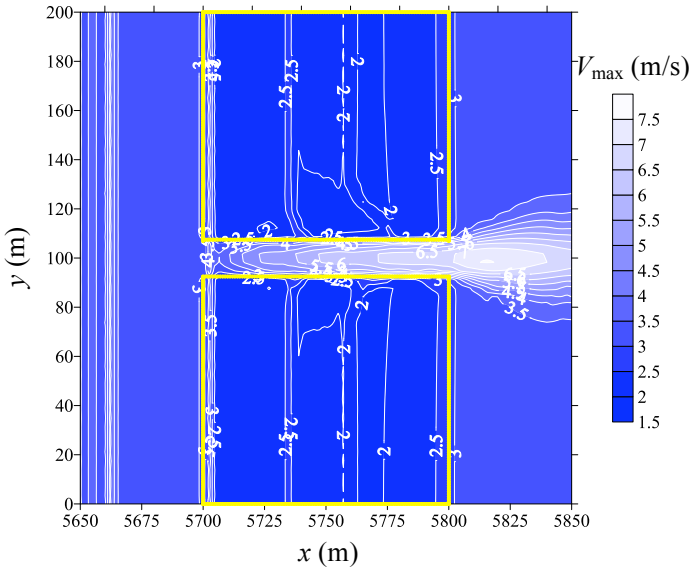

(a)

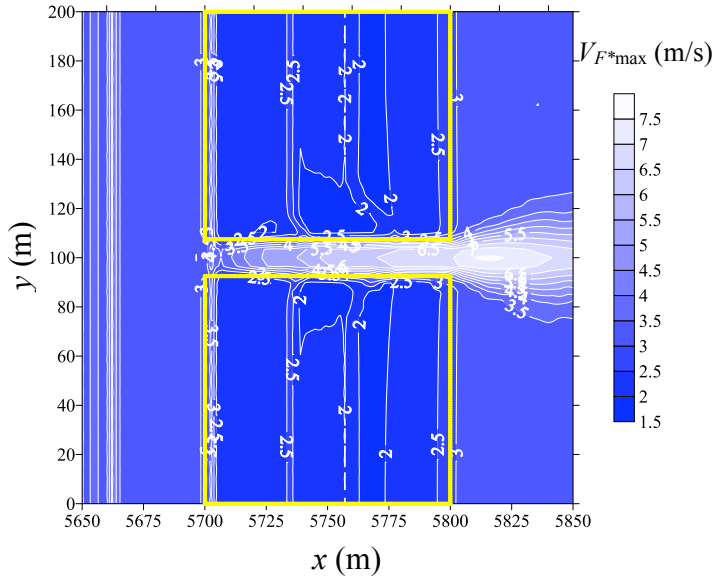

(b)

Fig. 12. Distribution of (a) maximum velocity (V_{max}), and (b) representative velocity (V_{F*max}).

Figs. 11-13 show that the contour line tends to become straight and parallel to the y-axis as the distance from the gap increases. This implies that the tsunami runup near the side boundaries is one-dimensional like the case with no gap. In the present paper, the representative checkpoints D and B were selected as corresponding to the case with no gap, although only a slight difference was apparent.

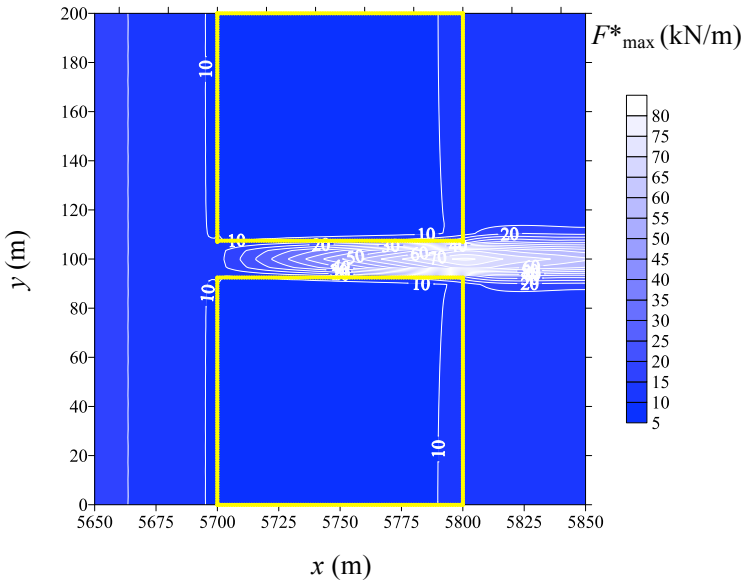

Fig. 13. Distribution of maximum tsunami force (F^*_{max}).

4.2.2. Effect of forest conditions

The tsunami force obtained by the incident tsunami condition of T=1200 s and H_{sl0}=6.94 m for different forest conditions were plotted in Fig. 14(a) and (b) against the following forest thickness B_{dNall}:

$$B_{dNall} = \gamma (1 \times B_F) b_{ref} C_{D-all} = \gamma B_F b^*_{ref} C_{D-all} \quad (18)$$

where, b_{ref} is the reference width per tree and b^*_{ref} is a logical reference width so that B_{dNall} has a unit of meters in the simple form (Note that b^*_{ref} has the same value as b_{ref} , but the unit is m^2/tree). The original form of forest thickness was proposed by Shuto (1987) for the combined effect of forest width and tree density. Tanaka et al. (2009) improved it to include resistance characteristic (C_{D-all}) due to the tree species as the upper expression in the right hand side of Eq.(18). In the present paper, the lower expression is used to make brief.

The forest width was changed with fixed tree density of 0.226 trees/m^2 and the tree density was changed with fixed forest width of 100 m. Tsunami forces F^*_{maxB}, F^*_{maxC} and F^*_{maxD} at points B, C and D decrease as the forest width and tree density increase due to mainly decrement of velocity with increase of forest resistance. On the other hand, the tsunami force F^*_{maxA} at point A is enhanced greatly but behaves in different ways by the forest width or tree density. This difference could be understood by the fact that the tsunami force with the increase of tree density increases to an extreme value corresponding to a rigid forest with the infinite density at the fixed point, while the tsunami force with the increase of forest width increases at first and then decreases to 0 finally because of the moving point. The enhancement of tsunami force at point A with the increase of density and width is due to the increase of velocity at the gap exit in spite of decrease of inundation depth as explained as the followings.

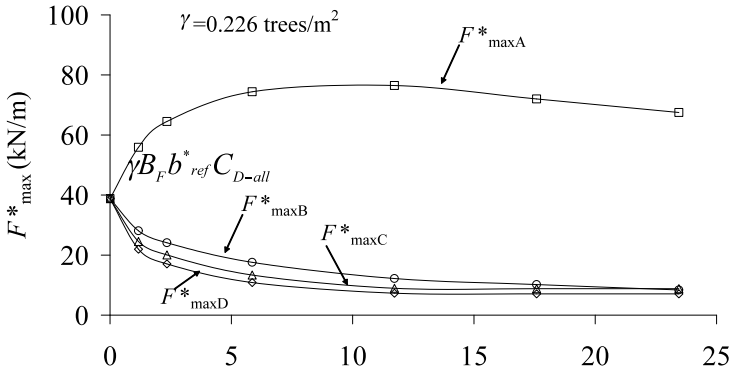

(a)

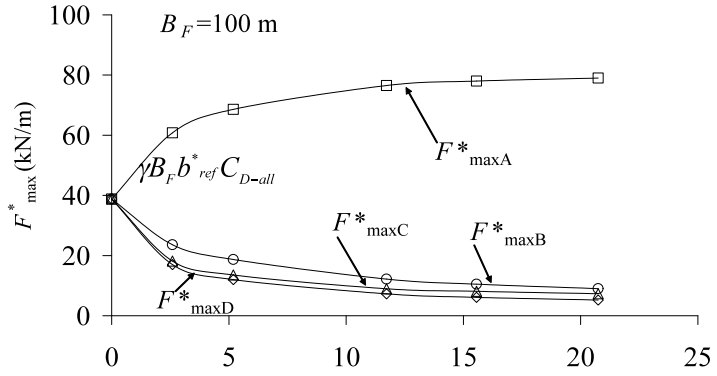

(b)

Fig. 14. Variation of tsunami force at A, B, C and D with (a) forest width (Series 1), (b) tree density (Series 2).

Fig. 15 (a) and (b) shows the variations of the representative velocity ($V_{F*\max}$) and total depth ($d_{F*\max}$) at the time of maximum tsunami force together with variations of average maximum discharge fluxes ($\overline{Q}_{in\max}$, $\overline{Q}_{out\max}$, and $\overline{Q}_{side\max}$) against the forest width and the tree density, respectively, where $Q_{in\max}$ and $Q_{out\max}$ are the maximum inflow and outflow at the gap inlet and exit, and $Q_{side\max}$ is the total inflow from both sides to the gap. The over-bar indicates the average discharge flux divided by the gap width. As the width and density increase, the inflow at the gap inlet decreases because of the increase of resistance of forest (in other word, the increase of reflection). In contrast, the outflow at the gap exit is increased slightly at first and does not decrease so much due to the increasing inflow from sides. On the other hand, the inundation depth behind the forest decreases due to the increase of forest resistance. Consequently, the representative velocity at the gap exit increases to result in the increase of tsunami force there. For the change of forest width, however, the point A moves as the forest width increases, while it is fixed in the change of density. Therefore the tsunami force decreases as the forest width becomes considerably wide and reduces to 0 as the forest width reaches to about 1000 m in the present condition.

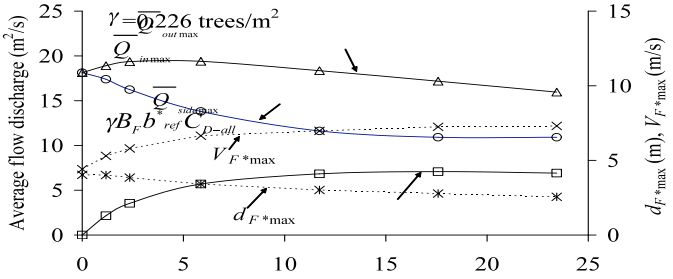

(a)

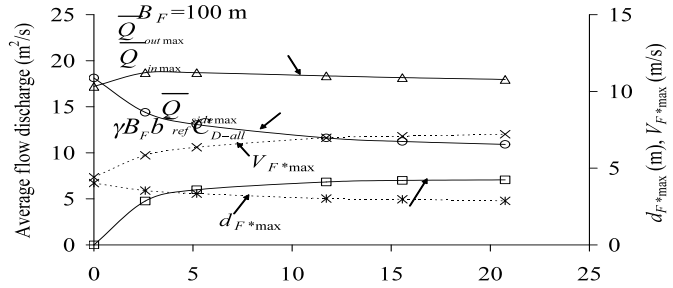

(b)

Fig. 15. Variation of representative water depth, representative velocity and maximum average discharge fluxes against (a) forest width (Series 1), (b) tree density (Series 2).

4.2.3. Effects of incident tsunami conditions

Fig. 16 (a) and (b) shows tsunami forces at four check points and the tsunami force F^*_{max0} in the case of no forest against the incident tsunami height and period. The conditions are B_F=100 m, γ=0.226 trees/m^2, T=1200 s (for the change of tsunami height) and H_{sl0}=6.94 m (for the change of tsunami period). The tsunami force in the case with no forest was taken at D, but it is almost the same with the tsunami force at B in the present forest condition. The tsunami force increases as the incident tsunami height increases. The relationship between the tsunami force and incident tsunami height can be expressed in the form of the following equation:

$$F^*_{max} = a_{Hf}\left(H_{sl0} - H_{cf}\right)^{b_{Hf}}, \quad H_{sl0} \geq H_{cf} \tag{19}$$

where H_{cf} is the threshold incident tsunami height at which the tsunami force becomes 0 and a_{Hf} has a dimension. In the present study, b_{Hf} was fixed as 2, because it may be reasonable to assume that tsunami force is proportional to the second power of the inundation depth and that the inundation depth is proportional to (H_{sl0}-H_{cf}). H_{cf} was also fixed as 2.5 m in the present study after considering the effect on the result and simplicity although, strictly speaking, it is a function of forest condition and tsunami period. The empirical constant of a_{Hf} is given in Fig.16 (a).

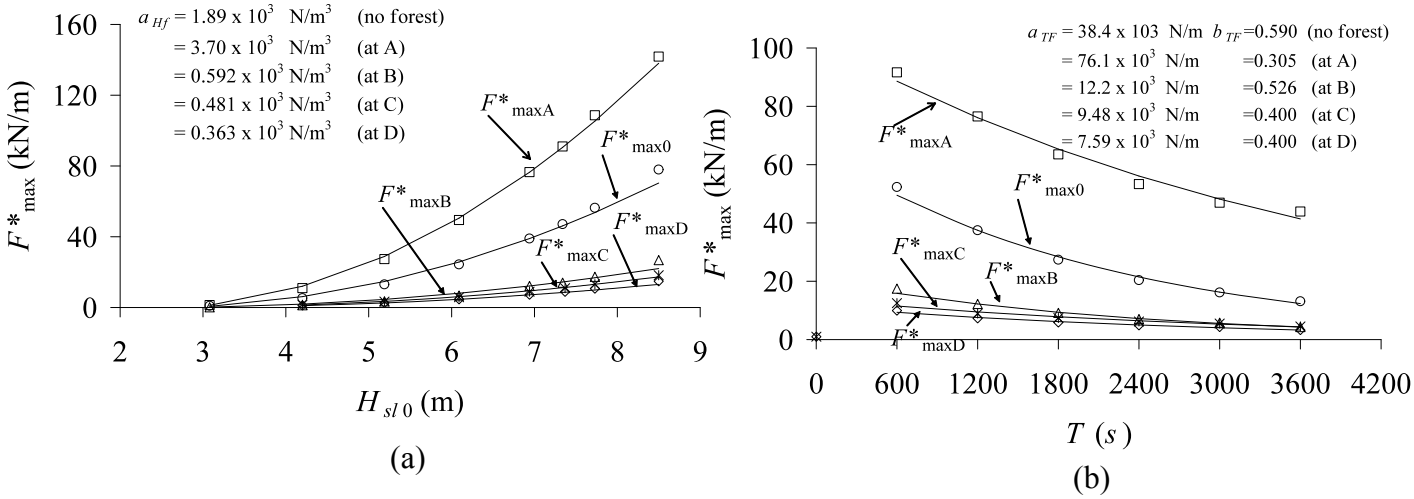

Fig. 16. Tsunami forces against (a) incident tsunami height (Series 3), and (b) tsunami period (Series 4).

On the other hand, the tsunami force decreases as the tsunami period increases in case of the fixed incident tsunami height. The relationship of the tsunami force and the tsunami period can be expressed in the form of the following equation:

$$F^*_{\max} = a_{Tf} \exp\left\{-b_{Tf}\left(\frac{T}{T_{rep}}-1\right)\right\} \tag{20}$$

where T_{rep} is the representative tsunami period and was taken as 1200 s in the present study, and a_{Tf} has a dimension. The determined empirical constants of a_{Tf} and b_{Tf} are given in Fig.16 (b). Both curve-fit relations against the incident tsunami height and period agree well with numerical results.

4.2.4. Non-dimensional tsunami forces for all simulation results

In the present paper, the following non-dimensional forest thickness combining forest and tsunami conditions is considered:

$$\frac{B_{dNall}}{T_{rep}\sqrt{gH_{rep}}} = \frac{\gamma B_F b^*_{ref} C_{D-all}\left(H_{rep}\right)}{T_{rep}\sqrt{gH_{rep}}} \tag{21}$$

where $T_{rep}\sqrt{gH_{rep}}$ corresponds to a wavelength of long waves with period of T_{rep} at the depth of H_{rep}. It should be noted, however, that the non-dimensional forest thickness represents the forest condition only, since the tsunami condition is fixed to the representative tsunami condition in Eq.(21). The representative tsunami height H_{rep} is arbitrary as well as the representative tsunami period T_{rep} and was taken as 7 m in the present study.

On the other hand, the tsunami force $F^*_{\max}$ is made dimensionless by the following relationship in consideration of the curve-fit equations in 4.2.3 as:

$$\frac{F^*_{\max}}{\rho g H_{sl0}{}^2} = \frac{a_f\left(H_{sl0}-H_{cf}\right)^{f_{Hf}} \exp\left\{-b_{Tf}\left(T/T_{rep}-1\right)\right\}}{\rho g H_{sl0}{}^2} \frac{F^*_{\max rep}}{a_f\left(H_{rep}-H_{cf}\right)^{f_{Hf}}} = \alpha_f f_{Hf} f_{Tf} \tag{22}$$

where $\rho g H_{sl0}{}^2$ (unit: N/m) corresponds to double the hydrostatic force acting on a virtual high wall per unit length by inundation depth of H_{sl0}, and $F^*_{\max rep}$ is the representative tsunami force by incident tsunami with the representative height H_{rep} and arbitrary period T. α_f, f_{Hf} and f_{Tf} are non-dimensional and expressed as follows:

$$\alpha_f = \frac{F^*_{\max rep}}{\rho g H_{rep}{}^2} = \frac{F^*_{\max}}{f_{Hf} f_{Tf} \rho g H_{sl0}{}^2} \tag{23}$$

$$f_{Hf} = \left(\frac{1 - H_{cf} / H_{sl0}}{1 - H_{cf} / H_{rep}} \right)^{b_{Hf}} = 2.42 \left(1 - \frac{2.5}{H_{sl0}} \right)^2 \tag{24}$$

$$f_{Tf} = \exp\left\{ - b_{Tf} \left(\frac{T}{T_{rep}} - 1 \right) \right\} \tag{25}$$

The empirical constant of b_{Tf} at A, B, C and D was determined based on the numerical results as:

$$\left.\begin{aligned} b_{Tf} &= 0.307 + 0.279 \exp\left(- 3.13 \times 10^3 \frac{\gamma B_F b^*_{ref} C_{D-all}\left(H_{rep}\right)}{T_{rep}\sqrt{g H_{rep}}} \right), && \text{at A} \\ &= 0.526, && \text{at B} \\ &= 0.400, && \text{at C and D} \end{aligned}\right\} \tag{26}$$

The empirical constant b_{Tf} at A is given as function of forest condition (B_F and γ), because the relation of tsunami force and forest condition is complex as shown in Fig.14 (a) and (b). The meaning of modification factors will be explained later.

All simulated results of non-dimensional value of α_f in Eq. (22) are plotted against the non-dimensional forest thickness of Eq. (21) in Fig. 17 (a) and (b). As being apprehensible by Eq. (23), f_{Hf} and f_{Tf} are modification factors so that the non-dimensional tsunami force is normalized to the non-dimensional tsunami force due to the incident tsunami with the representative height of H_{rep}. The α_f is called the normalized tsunami force. Due to the changes in tsunami conditions, many data were plotted at the same point on the abscissa, and some data are superimposed.

In Fig. 17(a) and (b), relationships calculated by the following curve-fit equations are shown:

$$\left.\begin{aligned} \alpha_f &= 0.164 - 0.0824 \exp\left(- 4.09 \times 10^3 \frac{\gamma B_F b^*_{rep} C_{D-all}\left(H_{rep}\right)}{T_{rep}\sqrt{g H_{rep}}} \right), && \text{at A} \\ &= 0.0794 \exp\left(- 0.0311 \times 10^3 \left[\frac{\gamma B_F b^*_{ref} C_{D-all}\left(H_{rep}\right)}{T_{rep}\sqrt{g H_{rep}}} \right]^{0.492} \right), && \text{at B} \\ &= 0.0186 + 0.0633 \exp\left(- 4.22 \times 10^3 \frac{\gamma B_F b^*_{ref} C_{D-all}\left(H_{rep}\right)}{T_{rep}\sqrt{g H_{rep}}} \right), && \text{at C} \\ &= 0.0139 + 0.0678 \exp\left(- 4.05 \times 10^3 \frac{\gamma B_F b^*_{ref} C_{D-all}\left(H_{rep}\right)}{T\sqrt{g H_{rep}}} \right), && \text{at D} \end{aligned}\right\} \tag{27}$$

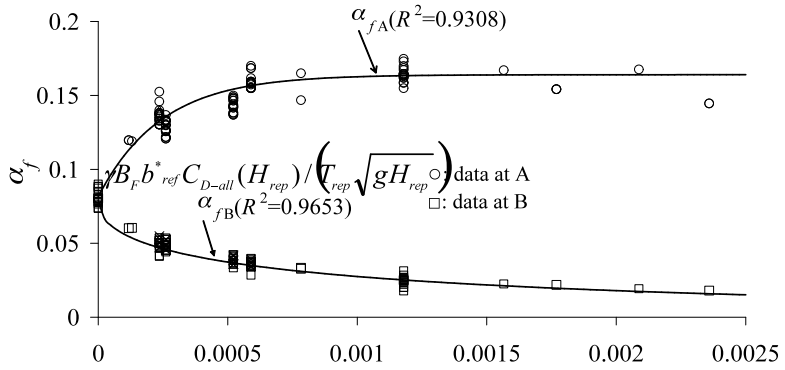

(a)

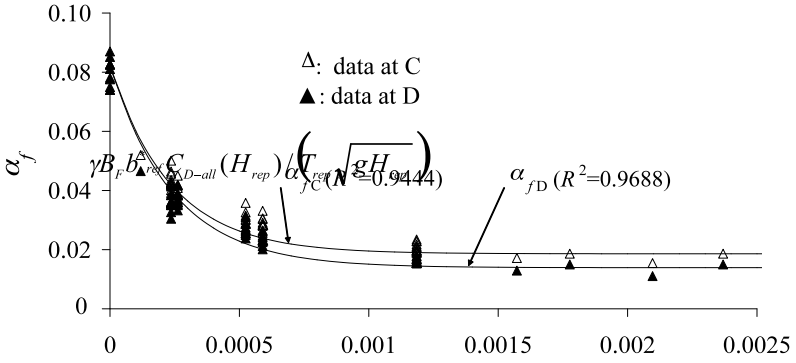

(b)

Fig. 17. Normalized tsunami force against non-dimensional forest thickness, (a) at A and B, (b) at C and D (Series 1-12).

In the figure, the relationships are indicated with the subscript A, B, C and D. Those curve-fit equations represent the average relationship of the non-dimensional tsunami force against non-dimensional forest thickness fairly well although the data are considerably scattered due to variety of conditions.

Fig. 18 shows the correlation of tsunami force at A, B, C and D estimated from the normalized tsunami force by Eq. (27) and tsunami force obtained by a numerical simulation with the absolute values. The agreement is fairly good. In the figure, the relations for y=1.1x and y=0.9x are also shown.

The error was within 10%. Eq. (27) can be applied to calculate tsunami force at A, B, C and D respectively if all information of forest and tsunami conditions are available. Note, however, that α_f at A is effective for the condition of B_F<200 m.

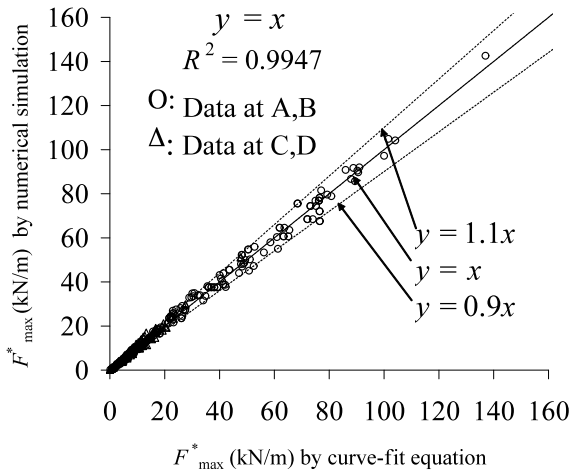

Fig. 18. Correlation of tsunami force by numerical simulations and by curve-fit equation at A, B, C and D (Series 1-12).

5. SUMMARY AND CONCLUSIONS

The summary and conclusions of the present study are as follows:

1. Laboratory experiments were carried out to validate the applicability of numerical model based on two-dimensional nonlinear long-wave equations including drag resistance of trees and turbulence induced shear forces to flow around a simplified forest model with a gap. It was confirmed that the water surface elevation and flow velocity by the numerical simulations agree well with the experimental results for various forest conditions of width and tree density.

2. The numerical model was applied to a prototype scale condition of a coastal forest of *Pandanus odoratissimus* with a gap to investigate the effects of forest conditions (width B_F and tree density γ) and incident tsunami conditions (period T and height at shoreline H_{sl0}) on a potential tsunami force which is defined as the total drag force on a virtual high column with unit width and unit drag coefficient. The potential tsunami force at the gap exit is greatly enhanced due to mainly the inflow to the gap through sides of vegetation patch and the maximum in the spatial distribution around and inside the forest, which reaches to twice of the potential tsunami force in the case of no forest in unfavorable conditions.

3. The potential tsunami forces at four representative points at front and back of forest including the center of gap exit were analyzed for various conditions and formulated as function of forest and tsunami conditions in the non-dimensional form. The potential tsunami forces at the gap exit increases as the increase of forest resistance due to the increase of forest width (B_F<100 m) and tree density, as the incident tsunami height increases and as the tsunami period decreases. The potential tsunami force at other points behind the vegetation patch and the front of forest decreases as the forest resistance increases. The potential tsunami forces calculated by the curve-fit formula in the non-dimensional form agree well with the simulated potential tsunami forces within ±10% error (B_F<200 m).

In the present paper, mature *P. odoratissimus* trees distributed uniformly in a forest were considered. However, tree conditions are not uniform in the actual forest and differ in the growth stage. To investigate the effects of non-uniform distribution of the various growth stages on tsunami forces is an exciting subject to be studied. Further, including the breaking of trees in numerical simulations is another subject of future study, as well as verification of the method of numerical simulations including tree breaking by field data.

ACKNOWLEDGEMENTS

This work was supported in part by JSPS AA Science Platform Program. The first author would like to acknowledge the financial support of the Government of Vietnam for his postgraduate study at Saitama University.

REFERENCES

Chakrabati, SK., 1991. Wave force on offshore structures. In: J.B. Herbich, Editor, Handbook of Coastal and Ocean engineering, Vol. 2 (1991), pp. 1-54.

Danielsen, F., Sorensen, M.K., Olwig, M.F., Selvam, V., Parish, F., Burgess, N.D., Hiraishi, T., Karunagaran, V.M., Rasmussen, M.S., Hansen, L.B., Quarto, A., Suryadiputra, N., 2005. The Asian tsunami: A protective role for coastal vegetation. Science 310, 643.

Fernando, H.J.S., Samarawickrama, S.P., Balasubramanian, S., Hettiarachchi, S.S.L., Voropayev, S., 2008. Effects of porous barriers such as coral reefs on coastal wave propagation. Journal of Hydro-environment Research 1, 187-194.

Harada, K., Imamura, F., 2005. Effects of coastal forest on tsunami hazard mitigation – A preliminary investigation, Tsunamis: Case studies and Resent Development, ed. K. Satake (Advances in natural and Technological Hazards Research, Springer) pp. 279-292.

Imamura, F., Shuto, N., Goto, C., 1998. Numerical simulation of the transoceanic propagation of tsunami. Proceedings of paper presented at the Sixth Congress of the Asian and Pacific Regional Division, Int. Assoc. Hydraul. Res., Kyoto, Japan.

Kathiresan, K., Rajendran, N., 2005. Coastal mangrove forests mitigated tsunami. Estuarine, Coastal and Shelf Science 65, 601-606.

Kerr, A.M., Baird, H.B., 2007. Natural barriers to natural disasters. BioScience. 57(2), 102-103.

Koh, H.L., Tek, S.Y., Liu, P.L., Ismail, A.I., Lee, H.L., 2008. Simulation of Andaman 2004 tsunami for assessing impact on Malaysia. Journal of Asian Earth Sciences 36, 74-83.

Liu, P.L., Cho, Y.S., Yoon, S.B., Seo S.N., 1994. Numerical simulations of the 1960 Chilean tsunami propagation and inundation at Hilo, Hawaii. In: M.I. El-Sabh, Editor, Recent Development in Tsunami Research, Kluwer Academic Publishers (1994), pp. 99–115.

Mascarenhas, A., Jayakumar, S., 2008. An environmental perspective of the post-tsunami scenario along the coast of Tamil Nadu, India: Role of sand dunes and forests. Journal of Environmental Management 89, 24-34.

Nadaoka, K., Yagi, H., 1998. Shallow-water turbulence modeling and horizontal larger eddy computation of river flow. Journal of Hydraulic Engineering 124(5), 493-500.

Nandasena, N. A. K., Tanaka, N., Tanimoto, K., 2008. Perspective of coastal vegetation patches with topography variations for tsunami protection in 2D-numerical modeling. Annual Journal of Hydraulic Engineering, JSCE 52, 133-38.

Shuto N., 1987. The effectiveness and limit of tsunami control forests. Coastal Engineering in Japan. 30(1), 143-153.

Tanaka, N., Sasaki, Y., Mowjood, M.I.M., Jinadasa, K.B.S.N., 2007. Coastal vegetation structures and their functions in tsunami protection: Experience of the recent Indian Ocean tsunami. Landscape and Ecological Engineering 3, 33-45.

Tanaka, N., 2009. Vegetation bioshields for tsunami mitigation: review of the effectiveness, limitations, construction, and sustainable management. Landscape and Ecological Engineering 5, 71-79.

Tanaka, N., Nandasena, N. A. K., Jinadasa, K. S. B. N., Sasaki, Y., Tanimoto, K. Mowjood, M. I. M., 2009. Developing effective vegetation bioshield for tsunami protection. Journal of Civil and Environmental Engineering Systems 26, 163-180.

Thuy, N.B., Tanimoto, K., Tanaka, N., Harada K., Iimura, K., 2009a. Effect of open gap in coastal forest on tsunami run-up – Investigations by experiment and numerical simulation. Ocean Engineering 36, 1258-1269.

Thuy, N.B., Tanaka, N., Tanimoto, K., Harada K., Iimura, K., 2009b. Tsunami flow behind the coastal forest with an open gap-effects of tsunami and tree condition. Proceedings of the 6th International Conference on Coastal Dynamic, Tokyo-Japan (CD-Rom). DOI No: 10.1142/9789814282475_0050

Titov, V.V., Synolakis, C.E., 1997. Extreme inundation flows during the Hokkaido Nansei-Oki tsunami. Geophys. Res. Lett. 24(11), 1315-1318.